Human-chimpanzee differences in a *FZD8* enhancer alter cell cycle dynamics in the developing neocortex

J. Lomax Boyd[1], Stephanie L. Skove[1], Jeremy P. Rouanet[1], Louis-Jan Pilaz[1], Tristan Bepler[2], Raluca Gordân[2,3], Gregory A. Wray[2,4,5], Debra L. Silver[1,6,7,8*]

[1]Department of Molecular Genetics and Microbiology, Duke University Medical Center, Durham, NC 27710 USA

[2]Center for Genomic and Computational Biology, Duke University, Durham, NC 27710 USA

[3]Department of Biostatistics and Bioinformatics, Duke University Medical Center, Durham, NC 27710 USA

[4]Department of Biology, Duke University, Durham, NC 27710 USA

[5]Department of Evolutionary Anthropology, Duke University, Durham, NC 27710 USA

[6]Department of Cell Biology, Duke University Medical Center, Durham, NC 27710 USA

[7]Department of Neurobiology, Duke University Medical Center, Durham, NC 27710 USA

[8]Duke Institute for Brain Sciences, Durham, NC 27710 USA

* Corresponding author: debra.silver@duke.edu

Running title:

Human-accelerated *FZD8* enhancer of corticogenesis

Summary

The human neocortex differs from that of other great apes in several notable regards including altered cell cycle, prolonged corticogenesis, and increased size [1-5]. While these evolutionary changes likely contributed to the origin of distinctively human cognitive faculties, their genetic basis remains almost entirely unknown. Highly conserved non-coding regions showing rapid sequence changes along the human lineage are candidate loci for the development and evolution of uniquely human traits. Several studies have identified human-accelerated enhancers [6-14], but none have linked an expression difference to a specific organismal trait. Here we report the discovery of a human-accelerated regulatory enhancer (*HARE5*) of *FZD8,* a receptor of the Wnt pathway implicated in brain development and size [15, 16]. Using transgenic mice, we demonstrate dramatic differences in human and chimpanzee *HARE5* activity, with human *HARE5* driving early and robust expression at the onset of corticogenesis. Similar to *HARE5* activity*, FZD8* is expressed in neural progenitors of the developing neocortex [17-19]. Chromosome conformation capture assays reveal *HARE5* physically and specifically contacts the core *Fzd8* promoter in the mouse embryonic neocortex. To assess the phenotypic consequences of *HARE5* activity, we generated transgenic mice in which *Fzd8* expression is under control of orthologous enhancers (*Pt-HARE5::Fzd8* and *Hs-HARE5::Fzd8*). In comparison to *Pt-HARE5::Fzd8*, *Hs-HARE5::Fzd8* mice showed marked acceleration of neural progenitor cell cycle and increased brain size. Changes in *HARE5* function unique to humans thus alter cell cycle dynamics of a critical population of stem cells during corticogenesis, and may underlie some distinctive anatomical features of the human brain.

Results

Identification of human-accelerated enhancer loci in the developing neocortex

The dramatic expansion of the neocortex during hominoid evolution is proposed to underlie the emergence of our uniquely human cognitive abilities [20-22], although strong genetic correlations between these traits have remained elusive [23]. The evolution of human cortical features, such as enlarged brain size, has been attributed to cellular changes including neuron number and neural progenitor cell cycle [1-5, 15]. However the genetic basis for these traits, which so markedly distinguish humans from other primates, remains poorly understood. Mutations within regulatory elements have been proposed to play a significant role in the evolution of human-specific traits [24, 25]. Recent genomic studies support this notion, and have collectively identified highly conserved non-coding regions that are rapidly evolving along the human lineage [6-10]. Of note, these human-accelerated noncoding loci are frequently located nearby genes implicated in brain development and function [11, 26, 27]. Together, these studies suggest the evolution of human neocortical traits may have occurred through modification of *cis*-regulatory enhancers involved in brain development. Yet to date just a handful of human-accelerated regions have been shown to function as forebrain enhancers [11-13] and none have been shown to impact neocortical expansion. Here we sought to discover human-accelerated regulatory loci important for corticogenesis, in order to gain insights into the genetic basis for the evolution of uniquely human brain features.

We identified *HARE5* from an *in silico* screen for rapidly evolving human noncoding regions predicted to function as developmental enhancers in the mammalian neocortex (Figure S1A, Table S1, Supplemental Experimental Procedures)[6-8, 28, 29]. Using a

standard mouse transient transgenic assay [11, 14], *HARE5* reporter activity was robust in the lateral neocortex and dorso-lateral midbrain (15/15 embryos) (Figures 1A, S1C). *HARE5* was prioritized due to this enhancer activity and its chromosomal location adjacent to *FRIZZLED8 (FZD8)*, a receptor for the Wnt signaling pathway implicated in neocortical development (Figure 1B)[15-18, 30, 31]. The *Homo sapiens (Hs) HARE5* orthologue contains 16 changes compared to *Pan troglodytes (Pt)*. Based on outgroup comparison, 10 mutations were fixed on the human branch and 6 on the chimpanzee branch since the latest common ancestor (Figure 1B). A phylogenetic analysis of the 1.2 Kb *HARE5* locus across several great ape species revealed a longer branch for the *Hs* orthologue compared to that of *Pt* (Figure 1C). This is consistent with the original signature of positive selection detected in the human relative to chimpanzee lineage [7]. Analysis of predicted transcription factor binding sites across the *HARE5* locus revealed differences, particularly at human-derived mutations, for key transcription factors relevant to corticogenesis (see Table S2) [32]. Together these results support the prediction that *Hs-HARE5* acquired unique enhancer activity since diverging from the common chimpanzee lineage.

Distinct enhancer activity of human and chimpanzee *HARE5* in the developing neocortex

We postulated that human and chimpanzee *HARE5* might differentially regulate gene expression during corticogenesis. To test this we generated independent stable mouse transgenic lines (*Pt-HARE5::LacZ* and *Hs-HARE5::LacZ*). Corticogenesis initiates at embryonic day (E) 9.5 and continues to E18.5 [2]. At E9.5, both *Pt-HARE5* and *Hs-*

HARE5 enhancer activity were undetectable (Figures 2A-C). However within a half day of development at E10.0, *Hs-HARE5* activity was rapidly and robustly upregulated in the lateral telencephalon (Figures 2E,F). In contrast, *Pt-HARE5* activity in the E10.0 telencephalon was markedly weaker and limited to more lateral regions (Figures 2D,F). This spatial difference in enhancer activity was sustained at E10.5, as evidenced by both whole mount embryos and coronal brain sections (Figures 2G-I, S2A-D). By E11.5, species-specific differences in *HARE5*-driven LacZ activity were still evident, although far less dramatic (Figures 2J-L). These results indicate that *HARE5* orthologues drive expression in the developing lateral telencephalon. However, relative to chimpanzee, the human enhancer has considerably earlier and robust activity during corticogenesis.

Having established spatial and temporal differences in chimpanzee and human *HARE5* enhancer activity, we next sought a more sensitive and dynamic readout of *HARE5* transcriptional activity. The LacZ protein is stable for at least 48 hours whereas destabilized fluorescent proteins with PEST motifs are only stable for 2 hours post-translation [33]. We generated new stable transgenic mouse lines, *Pt-HARE5*::*tdTomatoPEST* and *Hs-HARE5*::*EGFP-PEST*, and compared native fluorescence in embryos co-expressing the reporters (Figures 2M,N). Both orthologues drove enhancer activity in the E11.0 neocortex, however *Hs-HARE*::*EGFP* was considerably brighter than *Pt-HARE5*::*tdTomato*, despite tdTomato having intrinsically brighter fluorescent emission than EGFP (Figures 2N-T) [33]. This reporter difference was sustained at E12.5, though the chimpanzee enhancer remained active (Figures 2U-AA, S2E-H). We quantified enhancer activity by RT-qPCR measurement of reporter transcript levels in E12.5 neocortices. *Hs-HARE5*::*EGFP* embryos showed 10-30 fold higher

transcript levels than *Pt-HARE5*::*tdTomato* (Figure 2BB). Hence multiple independent reporter lines (LacZ and fluorescent) demonstrate that compared to chimpanzee *HARE5*, human *HARE5* drives dramatically higher enhancer activity in the telencephalon.

In the E10.5 telencephalon, the predominant neural progenitor populations are neuroepithelial cells, and by E12.5 these are replaced by radial glia (termed neural stem cells) [2]. At E10.5, both enhancers were active in the majority (about 75%) of Pax6-positive neuroepithelial cells and in some TuJ1-positive neurons (Figures S3I-U). At E12.5, reporter activity was highest in the ventricular zone (VZ) (Figure 2SE-H), where radial glial cells reside. Thus both human and chimpanzee *HARE5* enhancers are active in neural progenitors of the developing neocortex.

Chromosome conformation capture (3C) detects *HARE5-Fzd8* interactions

Having established *HARE5* activity within the lateral telencephalon, we next sought to identify the likely target gene. The most proximal gene, *Hs-FZD8*, is located 307,758 bps downstream from *HARE5* and was an obvious candidate due to its expression in the developing human and mouse neocortex [17-19, 30, 31]. LacZ reporter activity and *Fzd8 in situ* hybridization showed similar expression patterns in E10.5 and E11.5 whole mount embryos and neocortical sections (Figure S3)(developingmouse.brain-map.org and www.emouseatlas.org) [31]. We used chromosome conformation capture (3C) assays [34] to test for physical association between endogenous mouse (*Mm*) *HARE5* and the core *Fzd8* promoter within E12.5 mouse neocortices (Figure 3A). In neocortices we observed a strong peak of interaction between *Mm-HARE5* and the proximal *Fzd8* promoter, compared to flanking loci (Figure 3B). In contrast, no interactions were evident

between *Mm-HARE5* and *Fzd8* in age-matched liver, which lacks detectable *HARE5* activity and *Fzd8* expression. These data indicate *HARE5* physically and specifically associates with the core *Fzd8* promoter in the developing mouse neocortex. Given the *cis*-regulatory activity of *HARE5* orthologues, we propose *HARE5* functions as a distal-acting enhancer of *FZD8* during early human neocortical development.

Human HARE5 accelerates neural progenitor cell cycle and impacts neocortical size

We next assessed the functional consequences of chimpanzee and human *HARE5* activities during corticogenesis. We generated new independent transgenic mouse lines in which *Hs-HARE5* or *Pt-HARE5* drove expression of a MYC-tagged mouse *Fzd8* coding sequence (*Pt-HARE5*::*Fzd8* and *Hs-HARE5*::*Fzd8*) (Figure 4A). Expression of MYC in embryonic neocortices was confirmed by western blot analysis (Figure S4A). We postulated that *Fzd8* expression driven by the *HARE5* enhancer would impact the cell cycle state of neural progenitors based upon the following rationale. First, both *Hs-HARE5* and *Pt-HARE5* drive expression in neural progenitors. Second, modulating *Fzd8* levels impacts neural progenitor cell cycle in the retina [18]. Third, overexpression of stabilized β-catenin, a Wnt signaling component downstream of Frizzled, induces an expanded and gyrencephalic brain and slows cell cycle exit of neural stem cells in mice [15]. Fourth, cell cycle length is critical for corticogenesis and is postulated as a likely mechanism for the evolutionary expansion of the primate neocortex [35, 36].

We measured the cell cycle state of progenitors at E12.5, predicting that species-specific differences in *HARE5* activity would be evident within two days of onset of

enhancer activity. At this stage, radial glial progenitors primarily undergo symmetric divisions to expand laterally, but a subset divides asymmetrically to produce excitatory neurons [2]. Quantification of G2/M phases using phospho-histoneH3 (PH3) staining revealed a significant 1.3-fold increase in the proportion of total PH3+ cells in *Hs-HARE5*::*Fzd8* brains relative to both *Pt-HARE5*::*Fzd8* and non-transgenic wild-type (WT) littermates (Figures 4B-E). We also observed a trend towards more Pax6-positive radial glia in *Hs-HARE5*::*Fzd8* brains, with a significant increase relative to WT (Figure S4B). These snapshot measurements indicate that at E12.5 *Hs-HARE5* driven expression of *Fzd8* alters the proliferating population. More G2/M positive progenitors may indicate a faster overall cell cycle with similar G2/M phases, or alternatively an identical cell cycle with longer G2/M.

To help discriminate between these possibilities, we quantified cell cycle duration at E12.5. We used a paradigm of 2 hour BrdU exposure and 30 minute EdU exposure coupled with Ki67 staining, as previously described [37] (Figures 4F). Both WT and *Pt-HARE5*::*Fzd8* progenitors cycled for about 12 hours, as previously reported for this age [37, 38]. In contrast *Hs-HARE5* driven *Fzd8* expression significantly accelerated both the total cell cycle (to approximately 9.2 hours) and S phase, by 25% (Figures 4G-J, Table S3). These cell cycle differences correspond to a 23% shorter G1/G2/M duration (Tc-Ts) of *Hs-HARE5*::*Fzd8* progenitors compared to *Pt-HARE5*::*Fzd8* (P=0.003). Taken together, this functional analysis reveals that relative to both WT and *Pt-HARE5*::*Fzd8*, human *HARE5* directed expression of *Fzd8* accelerates neural progenitor cell cycle.

Increased proliferation of neural progenitors is frequently associated with changes in brain size. Therefore, we measured the cortical dimensions of transgenic E18.5 brains.

Compared to *Pt-HARE5*::*Fzd8* and WT, the dorsal area of *Hs-HARE5*::*Fzd8* cortices was significantly larger by 12% (Figures 4K-O). Across 5 additional measurements, *Hs-HARE5*::*Fzd8* cortices were consistently larger than both *Pt-HARE5*::*Fzd8* and WT (Figures S4F-H). As larger cortical area could be due to increased cortical thickness or tangential length, we quantified these dimensions in sagittal and coronal sections (Figures 4P-S). *Hs-HARE5*::*Fzd8* brains were thinner than *Pt-HARE5*::*Fzd8* and WT, although differences were only significant in comparison to WT (Figure S4I). In contrast, compared to both *Pt-HARE5*::*Fzd8* and WT, *Hs-HARE5*::*Fzd8* brains showed significantly longer tangential distance along the cortical VZ (Figure 4S). As seen in other mutants with longer tangential growth, *Hs-HARE5*::*Fzd8* brains also showed enlarged ventricles. The increased tangential length phenotype is often associated with greater progenitor proliferation and larger cortical size, as evidenced in mouse embryonic brains mis-expressing β-catenin or FGF2 [15, 39]. These data indicate that tangential expansion is a likely contributing factor for the increased cortical area.

We predicted faster progenitor proliferation would ultimately be associated with more neurons. To test this, we quantified the densities of FoxP1-positive neurons (mid-layers III-V), born between E13.5-E16.5, and FoxP2 neurons (deep-layer VI), born around E12.5 (Figures 4T-AA) within radial columns of E18.5 brains [40, 41]. Compared to chimpanzee, *Hs-HARE5*::*Fzd8* brains showed a significant 14% increase in the density of FoxP1 neurons, but no difference in FoxP2 neurons, nor any notable apoptosis. Thus, *Hs-HARE5*::*Fzd8* brains contain a higher density of neurons that are produced beginning around E13.5. Together these data indicate that, compared to *Pt-HARE5*, *Hs-HARE5*

promotes faster progenitor cell cycle, which is ultimately associated with increased Foxp1 excitatory neuron density, and overall larger cortical size.

Discussion

The neocortex expanded spectacularly during human evolution, giving rise to distinctively human anatomical and cognitive capabilities [1, 2, 20-22]. Yet to date, just a handful of genetic loci have been associated with human-specific brain traits [3, 5, 25], and none have been shown to functionally impact corticogenesis in an evolutionarily divergent fashion. In this study we report the discovery of the first human-accelerated enhancer that functions in brain development. We demonstrate dramatic temporal and spatial differences in activity of human and chimpanzee enhancers of *FZD8* during early corticogenesis, and show these differences impact neural progenitor cell cycle and brain size. Our study suggests the intriguing hypothesis that evolutionary changes in *HARE5* sequence and activity contributed to the origin of unique features of the human brain.

The evolutionarily divergent activities of *HARE5* support a model proposed 16 years ago by Pasko Rakic, that species differences in progenitor proliferation may contribute to distinctions in brain size between humans and non-human primates. The proposed radial unit hypothesis predicts that the number and proliferative capacity of progenitor cells drives the evolution of brain cytoarchitecture and explains species differences in neocortical size and structure [36]. Indeed both empirical and predicted measurements of neural progenitor cell cycle reveal stark differences between humans, non-human primates, and mice [1, 36, 42]. In non-human primates, distinct G1 phase durations are

associated with unique brain cytoarchitecture [35]. Moreover genetic evidence strongly supports a causal link between neural stem cell proliferation and human brain size [43].

How might a faster cell cycle impact human brain size? We speculate that in the context of extended human corticogenesis and gestation, *HARE5* increases progenitor proliferation, which expands the progenitor pool during early corticogenesis. Increased progenitor expansion would ultimately produce more neurons and a larger neocortex. This could involve either altering progenitor cell cycle exit and/or the division state of progenitors from neurogenic to proliferative. In E14.5 mice, proliferating and neurogenic neural progenitors have distinct S phase durations [44]. Experimentally shortening G1 phase in mice promotes proliferative divisions in lieu of neurogenic divisions, impacting neuron production [45, 46]. Our study implicates shorter G1 as a potential mechanism, as the Tc-Ts fraction was shorter in human transgenic brains. Follow-up studies of the *Hs-HARE5::Fzd8* mouse will clarify the detailed relationship between altered cell cycle and brain size, and elucidate if modifications in structural and behavioral traits exist.

We have shown that a key target gene of *HARE5* activity in the neocortex is *FZD8*, which encodes a Wnt receptor. Given the neurogenesis roles of β-catenin and Lef/Tcf, it is likely that *FZD8* acts via canonical Wnt signaling [16]. *FZD8* expression in the neonatal human brain is highest in cortical areas at 9 pcw (post conception weeks) (brainspan.org)[19] when neural stem cells are rapidly expanding during early corticogenesis [2], but markedly lower in non-cortical areas. The *FZD8* expression pattern correlates strongly with neural stem cell markers *SOX2* and *PAX6* ($r > 0.90$)[19, 47]. Hence the pattern of *HARE5* activity and *FZD8* expression is consistent with a functional relationship in neural stem cell regulation in humans. Although chimpanzee expression

data are not available, developing rhesus macaque (*Macaca mulatta*) neocortical data are (www.blueprintnhpatlas.org). Relative to 10 common transcripts of human and macaque developing neocortices, *FZD8* was more abundant in humans. As RNA expression data becomes available [48], it may become possible to more directly compare *FZD8* levels in human and non-human primates.

In addition to its requirement for early mouse corticogenesis, Wnt signaling is implicated in human brain traits. In 2002 Chenn et al. showed that expression of stabilized β-catenin induced a larger, gyrencephalic phenotype reminiscent of the human brain [15]. However, evidence for the involvement of this pathway in human brain evolution has remained elusive until now. Our identification of *HARE5* highlights the transcriptional regulation of Wnt signaling components as a new avenue to explore for understanding the evolutionary origin of human specific anatomical and cognitive traits. With the ability to identify regulatory elements active during development [49], we are now poised for the discovery of additional loci and pathways whose modification provided the underpinnings for the evolution of the human brain.

Author Contributions

JLB, GAW, and DLS conceived the study and wrote the paper. JLB, SLS, JPR, LJP, TB, RG, and DLS performed and analyzed experiments.

Acknowledgements

We thank the following: Dr. Len Pennacchio, Dr. Jérôme Collignon, Dr. Jeremy Nathans and Dr. Yanshu Wang for sharing reagents; Meilang Flowers and Cheryl Bock

(Duke Transgenic Mouse Facility) for generating mouse transgenics; Autumn Rorrer for assistance with mouse husbandry; Dr. Hiro Matsunami for reading the manuscript; members of the DLS and GAW labs for helpful discussions; Han-Yu Shih for advice on 3C analysis; EM for assistance with western blotting; DLS lab members for assistance in blind scoring of phenotypes. Funding from a Research Incubator grant from the Duke Institute for Brain Sciences (to DLS and GAW), by R01NS083897 (to DLS), and by NSF HOMIND BCS-08-27552 (to GAW).

References

1. Geschwind, D. H., and Rakic, P. (2013). Perspective. Neuron *80*, 633–647.

2. Lui, J. H., Hansen, D. V., and Kriegstein, A. R. (2011). Development and evolution of the human neocortex. Cell *146*, 18–36.

3. Enard, W., Gehre, S., Hammerschmidt, K., HOlter, S. M., Blass, T., Somel, M., BrUckner, M. K., Schreiweis, C., Winter, C., Sohr, R., et al. (2009). A Humanized Version of Foxp2 Affects Cortico-Basal Ganglia Circuits in Mice. Cell *137*, 961–971.

4. Herculano-Houzel, S. (2012). The remarkable, yet not extraordinary, human brain as a scaled-up primate brain and its associated cost. Proceedings of the National Academy of Sciences *109 Suppl 1*, 10661–10668.

5. Dennis, M. Y., Nuttle, X., sudmant, P. H., antonacci, F., Graves, T. A., Nefedov, M., Rosenfeld, J. A., Sajjadian, S., malig, M., Kotkiewicz, H., et al. (2012). Evolution of Human-Specific Neural SRGAP2 Genes by Incomplete Segmental

Duplication. Cell, 1–11.

6. Prabhakar, S., Noonan, J. P., Pääbo, S., and Rubin, E. M. (2006). Accelerated evolution of conserved noncoding sequences in humans. Science *314*, 786.

7. Bird, C. P., Stranger, B. E., Liu, M., Thomas, D. J., Ingle, C. E., Beazley, C., Miller, W., Hurles, M. E., and Dermitzakis, E. T. (2007). Fast-evolving noncoding sequences in the human genome. Genome Biol *8*, R118.

8. Lindblad-Toh, K., Garber, M., Zuk, O., Lin, M. F., Parker, B. J., Washietl, S., Kheradpour, P., Ernst, J., Jordan, G., Mauceli, E., et al. (2011). A high-resolution map of human evolutionary constraint using 29 mammals. Nature *478*, 476–482.

9. Bush, E. C., and Lahn, B. T. (2008). A genome-wide screen for noncoding elements important in primate evolution. BMC Evol. Biol. *8*, 17.

10. Pollard, K. S., Salama, S. R., King, B., Kern, A. D., Dreszer, T., Katzman, S., Siepel, A., Pedersen, J. S., Bejerano, G., Baertsch, R., et al. (2006). Forces shaping the fastest evolving regions in the human genome. PLoS Genet *2*, e168.

11. Capra, J. A., Erwin, G. D., McKinsey, G., Rubenstein, J. L. R., and Pollard, K. S. (2013). Many human accelerated regions are developmental enhancers. Philosophical Transactions of the Royal Society B: Biological Sciences *368*, 20130025.

12. Kamm, G. B., López-Leal, R., Lorenzo, J. R., and Franchini, L. F. (2013). A fast-evolving human NPAS3 enhancer gained reporter expression in the developing

forebrain of transgenic mice. Philosophical Transactions of the Royal Society B: Biological Sciences *368*, 20130019.

13. Oksenberg, N., Stevison, L., Wall, J. D., and Ahituv, N. (2013). Function and regulation of AUTS2, a gene implicated in autism and human evolution. PLoS Genet *9*, e1003221.

14. Prabhakar, S., Visel, A., Akiyama, J. A., Shoukry, M., Lewis, K. D., Holt, A., Plajzer-Frick, I., Morrison, H., FitzPatrick, D. R., Afzal, V., et al. (2008). Human-Specific Gain of Function in a Developmental Enhancer. Science *321*, 1346–1350.

15. Chenn, A., and Walsh, C. A. (2002). Regulation of cerebral cortical size by control of cell cycle exit in neural precursors. Science *297*, 365–369.

16. Freese, J. L., Pino, D., and Pleasure, S. J. (2010). Wnt signaling in development and disease. Neurobiology of Disease *38*, 148–153.

17. Fischer, T., Guimera, J., Wurst, W., and Prakash, N. (2007). Distinct but redundant expression of the Frizzled Wnt receptor genes at signaling centers of the developing mouse brain. Neuroscience *147*, 693–711.

18. Liu, C., Bakeri, H., Li, T., and Swaroop, A. (2012). Regulation of retinal progenitor expansion by Frizzled receptors: implications for microphthalmia and retinal coloboma. Hum Mol Genet *21*, 1848–1860.

19. Miller, J. A., Ding, S.-L., Sunkin, S. M., Smith, K. A., Ng, L., Szafer, A., Ebbert, A.,

Riley, Z. L., Royall, J. J., Aiona, K., et al. (2014). Transcriptional landscape of the prenatal human brain. Nature, 1–19.

20. Berwick, R. C., Friederici, A. D., Chomsky, N., and Bolhuis, J. J. (2013). Evolution, brain, and the nature of language. Trends in Cognitive Sciences *17*, 91–100.

21. Whiten, A. (2011). The scope of culture in chimpanzees, humans and ancestral apes. Philosophical Transactions of the Royal Society B: Biological Sciences *366*, 997–1007.

22. Shettleworth, S. J. (2012). Modularity, comparative cognition and human uniqueness. Philosophical Transactions of the Royal Society B: Biological Sciences *367*, 2794–2802.

23. Schoenemann, P. T. (2006). Evolution of the Size and Functional Areas of the Human Brain. Annu. Rev. Anthropol. *35*, 379–406.

24. King, M. C., and Wilson, A. C. (1975). Evolution at two levels in humans and chimpanzees. Science *188*, 107–116.

25. Bae, B.-I., Tietjen, I., Atabay, K. D., Evrony, G. D., Johnson, M. B., Asare, E., Wang, P. P., Murayama, A. Y., Im, K., Lisgo, S. N., et al. (2014). Evolutionarily dynamic alternative splicing of GPR56 regulates regional cerebral cortical patterning. Science *343*, 764–768.

26. Haygood, R., Babbitt, C. C., Fedrigo, O., and Wray, G. A. (2010). Contrasts

between adaptive coding and noncoding changes during human evolution. Proceedings of the National Academy of Sciences *107*, 7853–7857.

27. Johnson, M. B., Kawasawa, Y. I., Mason, C. E., Krsnik, Z., Coppola, G., BogdanoviC, D., Geschwind, D. H., Mane, S. M., State, M. W., and Sestan, N. (2009). Functional and Evolutionary Insights into Human Brain Development through Global Transcriptome Analysis. Neuron *62*, 494–509.

28. Creyghton, M. P., Cheng, A. W., Welstead, G. G., Kooistra, T., Carey, B. W., Steine, E. J., Hanna, J., Lodato, M. A., Frampton, G. M., Sharp, P. A., et al. (2010). Histone H3K27ac separates active from poised enhancers and predicts developmental state. Proceedings of the National Academy of Sciences *107*, 21931–21936.

29. Visel, A., Blow, M. J., Li, Z., Zhang, T., Akiyama, J. A., Holt, A., Plajzer-Frick, I., Shoukry, M., Wright, C., Chen, F., et al. (2009). ChIP-seq accurately predicts tissue-specific activity of enhancers. Nature *457*, 854–858.

30. Kim, A. S., Lowenstein, D. H., and Pleasure, S. J. (2001). Wnt receptors and Wnt inhibitors are expressed in gradients in the developing telencephalon. Mech Dev *103*, 167–172.

31. Summerhurst, K., Stark, M., Sharpe, J., Davidson, D., and Murphy, P. (2008). 3D representation of Wnt and Frizzled gene expression patterns in the mouse embryo at embryonic day 11.5 (Ts19). Gene Expression Patterns *8*, 331–348.

32. Berger, M. F., Philippakis, A. A., Qureshi, A. M., He, F. S., Estep, P. W., and

Bulyk, M. L. (2006). Compact, universal DNA microarrays to comprehensively determine transcription-factor binding site specificities. Nat. Biotechnol. *24*, 1429–1435.

33. Shaner, N. C., Steinbach, P. A., and Tsien, R. Y. (2005). A guide to choosing fluorescent proteins. Nat Methods *2*, 905–909.

34. Hagège, H., Klous, P., Braem, C., Splinter, E., Dekker, J., Cathala, G., de Laat, W., and Forné, T. (2007). Quantitative analysis of chromosome conformation capture assays (3C-qPCR). Nat Protoc *2*, 1722–1733.

35. Lukaszewicz, A., Savatier, P., Cortay, V., Giroud, P., Huissoud, C., Berland, M., Kennedy, H., and Dehay, C. (2005). G1 phase regulation, area-specific cell cycle control, and cytoarchitectonics in the primate cortex. Neuron *47*, 353–364.

36. Rakic, P. (1988). Specification of cerebral cortical areas. Science *241*, 170–176.

37. Martynoga, B. S., Morrison, H., Price, D. J., and Mason, J. O. (2005). Foxg1 is required for specification of ventral telencephalon and region-specific regulation of dorsal telencephalic precursor proliferation and apoptosis. Dev Biol *283*, 113–127.

38. Takahashi, T., Nowakowski, R. S., and Caviness, V. S. (1995). The cell cycle of the pseudostratified ventricular epithelium of the embryonic murine cerebral wall. J Neurosci *15*, 6046–6057.

39. Rash, B. G., Tomasi, S., Lim, H. D., Suh, C. Y., and Vaccarino, F. M. (2013). Cortical Gyrification Induced by Fibroblast Growth Factor 2 in the Mouse Brain.

Journal of Neuroscience *33*, 10802–10814.

40. Ferland, R. J., Cherry, T. J., Preware, P. O., Morrisey, E. E., and Walsh, C. A. (2003). Characterization of Foxp2 and Foxp1 mRNA and protein in the developing and mature brain. J Comp Neurol *460*, 266–279.

41. Greig, L. C., Woodworth, M. B., Galazo, M. J., Padmanabhan, H., and Macklis, J. D. (2013). Molecular logic of neocortical projection neuron specification, development and diversity. Nature Publishing Group *14*, 755–769.

42. Kornack, D. R., and Rakic, P. (1998). Changes in cell-cycle kinetics during the development and evolution of primate neocortex. Proc Natl Acad Sci USA *95*, 1242–1246.

43. Mirzaa, G. M., Parry, D. A., Fry, A. E., Giamanco, K. A., Schwartzentruber, J., Vanstone, M., Logan, C. V., Roberts, N., Johnson, C. A., Singh, S., et al. (2014). De novo CCND2 mutations leading to stabilization of cyclin D2 cause megalencephaly-polymicrogyria-polydactyly-hydrocephalus syndrome. Nat Genet *46*, 510–515.

44. Arai, Y., Pulvers, J. N., Haffner, C., Schilling, B., Nüsslein, I., Calegari, F., and Huttner, W. B. (2011). Neural stem and progenitor cells shorten S-phase on commitment to neuron production. Nature Communications *2*, 154.

45. Pilaz, L.-J., Patti, D., Marcy, G., Ollier, E., Pfister, S., Douglas, R. J., Betizeau, M., Gautier, E., Cortay, V., Doerflinger, N., et al. (2009). Forced G1-phase reduction alters mode of division, neuron number, and laminar phenotype in the cerebral

cortex. Proceedings of the National Academy of Sciences *106*, 21924–21929.

46. Lange, C., Huttner, W. B., and Calegari, F. (2009). Cdk4/cyclinD1 overexpression in neural stem cells shortens G1, delays neurogenesis, and promotes the generation and expansion of basal progenitors. Cell stem cell *5*, 320–331.

47. Lui, J. H., Nowakowski, T. J., Pollen, A. A., Javaherian, A., Kriegstein, A. R., and Oldham, M. C. (2014). Radial glia require PDGFD–PDGFRβ signalling in human but not mouse neocortex. Nature *515*, 264–268.

48. Pollen, A. A., Nowakowski, T. J., Shuga, J., Wang, X., Leyrat, A. A., Lui, J. H., Li, N., Szpankowski, L., Fowler, B., Chen, P., et al. (2014). Low-coverage single-cell mRNA sequencing reveals cellular heterogeneity and activated signaling pathways in developing cerebral cortex. Nat. Biotechnol. *32*, 1053–1058.

49. Visel, A., Taher, L., Girgis, H., May, D., Golonzhka, O., Hoch, R. V., McKinsey, G. L., Pattabiraman, K., Silberberg, S. N., Blow, M. J., et al. (2013). A High-Resolution Enhancer Atlas of the Developing Telencephalon. Cell *152*, 895–908.

Figure Legends

Figure 1. Identification of *Hs-HARE5* as a human-accelerated neocortical enhancer. (A) Representative E14.5 *Hs-HARE5*::*LacZ* embryo stained for β-galactosidase (LacZ) activity. (B) Schematic of *Hs-HARE5* locus on human chromosome 10 (hg19). The 1,219 bp long *HARE5* genomic locus with enhancer activity includes the original 619 bp human-

accelerated sequence and flanking 5' and 3' sequences. Represented below is a PhastCons conservation track for the *HARE5* locus, shown with the region of high conservation (grey). Also shown are lineage-specific mutations for chimpanzee (6, arrows, above line), and human (10, arrowheads, bottom), including 1 Denisovan (red) and 1 currently identified human polymorphism (blue). (C) Maximum likelihood phylogenetic tree for the *HARE5* orthologous locus from five anthropoid primates. Scale bars, 2 mm (A). See also Figure S1 and Table S1.

Figure 2. *Hs-HARE5* activity drives robust, early enhancer activity relative to *Pt-HARE5* during corticogenesis. (A-L) Developmental time-series of *Pt-HARE5*::*LacZ* (A,D,G,J) and *Hs-HARE5*::*LacZ* (B,E,H,K) reporter activity from stable transgenic lines. Representative images of LacZ stained embryos from lateral (top) and anterior (bottom) views. (C,F,I,L) Enhancer activity was qualitatively scored in the telencephalon, using the indicated scoring schema shown on the right, on a scale from no reporter activity (score 0) to full telencephalic activity (score 5). Number of embryos and independent transgenic lines analyzed for each stage are listed below. Embryos were scored blindly and independently by at least three individuals. (M) Schematic of destabilized reporter constructs drawn to scale. (N-AA) Representative embryos from dual reporter transgenic *Pt-HARE5::tdTomato*; *Hs-HARE5::EGFP* E11.0 (N-T) and E12.5 (U-AA) embryos detected by brightfield (N,U), and endogenous fluorescence for tdTomato (O,Q,S,V,X,Z) and EGFP (P,R,T,W,Y,AA) channels. Dotted lines demarcate dorsal neocortices of whole mount embryos (N-P, U-W). (Q,R,X,Y) Coronal sections from mid-cortex (plane indicated

by arrowhead in N,U) in tdTomato (Q,X) and EGFP (R,Y) channels. (S,T,Z,AA) High-magnification images of the lateral telencephalon for tdTomato (S,Z) and EGFP (T,AA). The number of embryos and lines for each analysis is listed beside U. Endogenous fluorescence images were captured using identical exposure conditions. (BB) Graph depicting log fold changes for RT-qPCR from E12.5 neocortices. Each data point is the average fold change for an individual *Hs-HARE5::EGFP* embryo relative to the aggregated average for all *Pt-HARE5::tdTomato* embryos. mRNA input levels were normalized to *Gapdh.* n=4 technical replicates per embryo; n=9 embryos from 3 transgenic lines from each genotype. Scale bars, 1 mm (A-K), 500 μm (N-P, U-W); 150 μm (Q,R,X,Y); 25 μm (S,T,Z,AA). See also Figure S2 and Table S2.

Figure 3. 3C analysis showing *HARE5* physically contacts the *Fzd8* promoter. (A) Schematic of 3C protocol showing *HARE5* and *Fzd8* loci (black bars), with indicated TaqMan probe (blue bar), test primers (black half arrows), and *HindIII* restriction sites (red lines). (B) 3C assay of E12.5 mouse neocortices (blue dots) and liver control tissue (red dots). Dark vertical line indicates location of TaqMan probe and constant primer anchored within the *Mm-HARE5* locus. The 0 position indicates ATG of *Fzd8* coding sequence. The graph depicts the relative frequency of interactions between *Mm-HARE5* and 6 genomic locations. See also Figure S3.

Figure 4. *Hs-HARE5* driven expression of *Fzd8* accelerates cell cycle of neural

progenitors, and increases neuron number and neocortical size. (A) Schematic of *Pt-HARE5::Fzd8* and *Hs-HARE5::Fzd8* constructs. (B-I) Images of coronal sections from E12.5 WT littermate (B,G), *Pt-HARE::Fzd8* (C,H), and *Hs-HARE5::Fzd8* (D,I) transgenic cortices. Sections stained for (B-D) PH3 (green) and Hoechst (blue), (G-I) BrdU (green) and EdU (red). (E) Graph of WT (white), *Pt-HARE::Fzd8* (grey), and *Hs-HARE5::Fzd8* (black) depicting percentage of all cells that are PH3-positive. (F) Paradigm for analysis of cell cycle length using double pulse of BrdU and EdU. Nucleotide analogs were injected at indicated time-points and overall cell cycle length (Tc) and S phase length (Ts) were calculated as shown. (J) Graph of WT (white), *Pt-HARE::Fzd8* (grey), and *Hs-HARE5::Fzd8* (black) cell cycle lengths of cycling progenitors. (K-M) Whole mount E18.5 brains from indicated genotypes with n=number of brains examined. A dotted line was drawn on WT cortex in K to indicate dorsal cortical area, and then superimposed on transgenic cortices in L and M. (N) Schematic cartoon representation of E18.5 brain with indicated regions of analyses for sagittal sections (P-S) and coronal sections (T-AA). (O) Graph of WT (white), *Pt-HARE::Fzd8* (grey), and *Hs-HARE5::Fzd8* (black) dorsal cortical area measurements. Note a 12% increase was seen in *Hs-HARE5::Fzd8* cortical area. (P-R) Sagittal E18.5 sections from brains of indicated genotypes. A line drawn on WT cortex in P indicates ventricular length, and was superimposed on transgenic cortices in Q and R. Note no evidence of cortical gyrification was seen. (S) Graph depicting ventricular length for indicated genotypes. (T-V, X-Z) Coronal E18.5 sections from neocortices of indicated genotypes and stained for Foxp1 (T-V) and Foxp2 (X-Z). Note no significant apoptosis was observed. (W, AA) Graphs depicting densities of Foxp1 (W) and Foxp2 (AA) neurons in radial columns of neocortical sections. The following were

analyzed for each genotype: for B-E, n=5 embryos each from 3 transgenic lines; for F-J, 5-7 embryos each from 2-3 transgenic lines; K-O, 16-57 embryos each from 2-3 transgenic lines; P-S, 4-5 embryos each (2-5 sections per embryo) from 2-3 transgenic lines; T-AA, 5-6 embryos each (2-4 sections per embryo) from 2-3 transgenic lines. All analyses were done blind to genotype. Error bars, s.d., *, $P < 0.05$, **, $P<0.01$, ***, $P<0.001$. Scale bars, 25 μm (B-I), 1 mm (K-M), 500 μm (P-R), and 100 μm (T-Z). See also Figure S4 and Table S3.

Supplemental Data

A

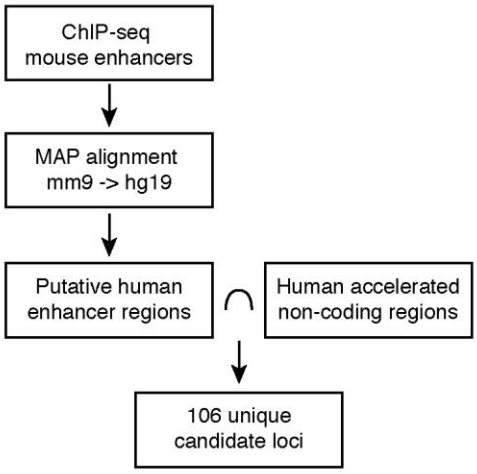

B

Human enhancer	*Hs-HARE1*	*Hs-HARE2*	*Hs-HARE3*	*Hs-HARE4*	*Hs-HARE5*	*Hs-HARE6*
Selection scan	Prabhakar	Bird	Prabhakar, Bird	Prabhakar	Bird	Lindblad-Toh
Chip-seq	H3K4me1	P300	P300	P300	P300	H3K4me1
Forebrain expression / total LacZ+	3/6	2/9	7/18	0/3	15/15	9/12

E14.5

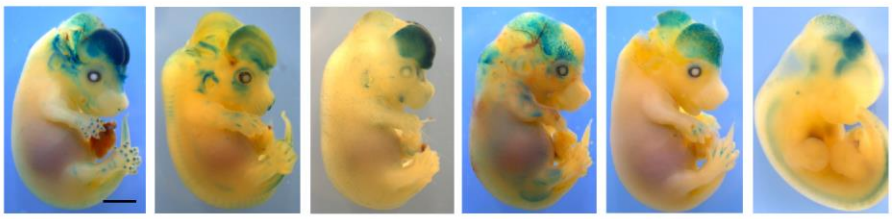

C *Hs-HARE5::LacZ* E14.5

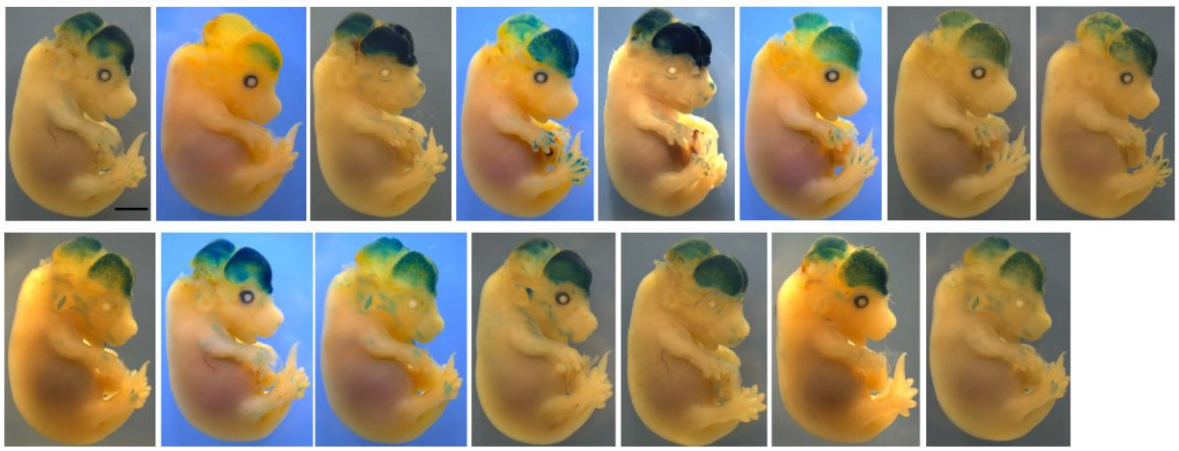

Figure S1, Related to Figure 1. **Screen for evolutionarily important enhancers.** (A) Schematic workflow for identifying human-accelerated brain enhancers, as described in Supplemental Experimental Procedures. 106 unique putative neocortical enhancer loci with signatures of positive selection were identified from the screen (see also Table S1). (B) Images of E14.5 representative transient transgenic embryos for *HARE1-6* assayed for β-galactosidase activity, and listed with relevant information. *HARE1*-6 were prioritized from the screen based on their proximity to genes known or predicted to be involved in corticogenesis. Selection scans are from following references (first author name listed): human-accelerated conserved noncoding sequence [S1]; accelerated conserved noncoding sequence [S2]; and primate accelerated region [S3]. Chip-Seq are from the following references: H3K4me1 [S4], P300 [S5]. *HAREs1, 2,* and *4* showed variable enhancer activity, whereas *HAREs 3, 5*, and *6* demonstrated more consistent LacZ enhancer activity. C) Images of E14.5 transient transgenic embryos for *Hs-HARE*5::*LacZ* assayed for β-galactosidase activity. Note *HARE5* activity in the lateral forebrain and dorso-lateral midbrain, and to a lesser and more variable extent in the spinal cord and retina. Scale bars, 2mm.

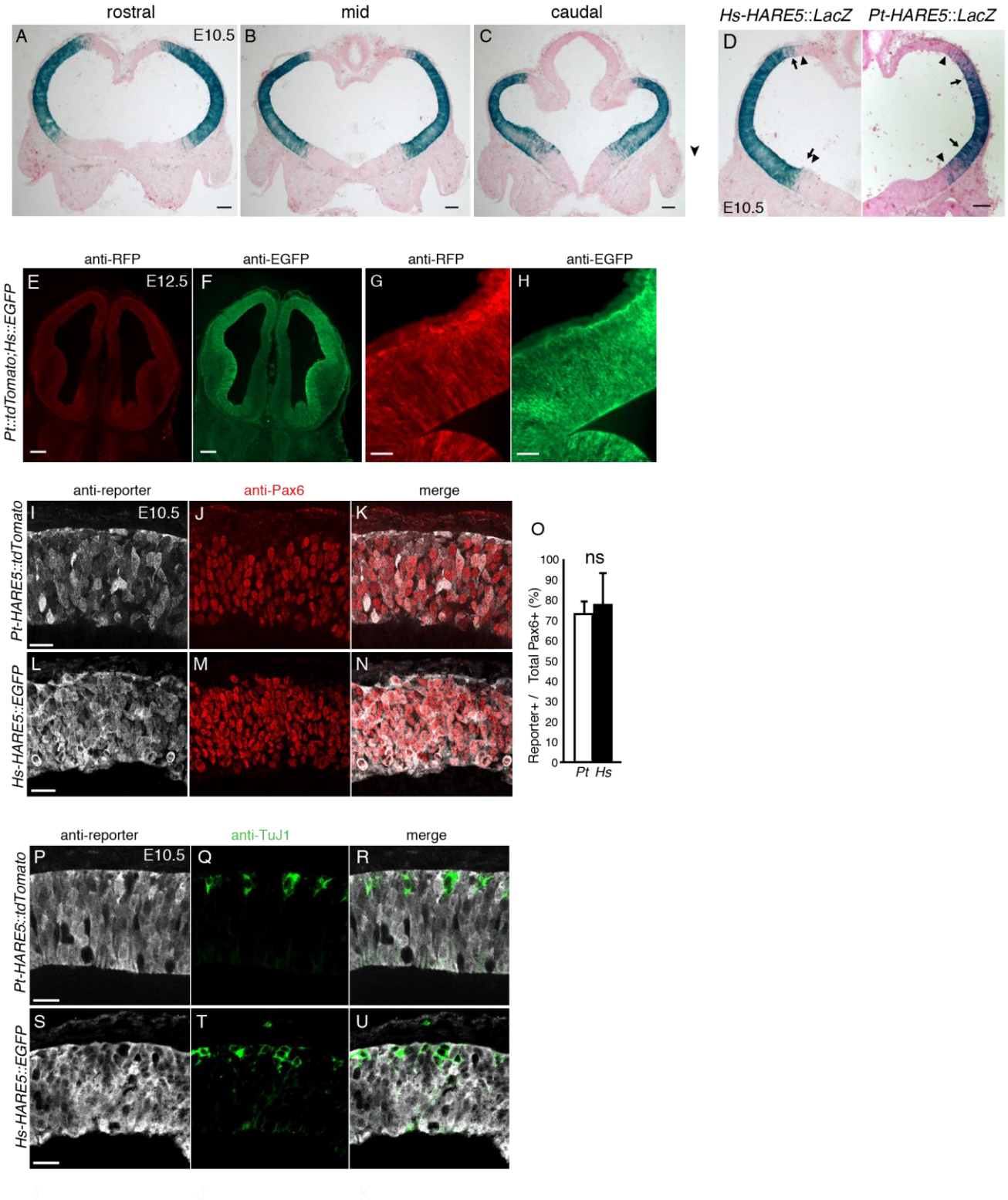
rostral
mid
caudal
A
E10.5
B
C
Hs-HARE5::LacZ
Pt-HARE5::LacZ
D
E10.5
anti-RFP
anti-EGFP
anti-RFP
anti-EGFP
Pt::tdTomato;Hs::EGFP
E
E12.5
F
G
H
anti-reporter
anti-Pax6
merge
Pt-HARE5::tdTomato
I
E10.5
J
K
Hs-HARE5::EGFP
L
M
N
O
ns
Reporter+ / Total Pax6+ (%)
100
90
80
70
60
50
40
30
20
10
0
Pt
Hs
anti-reporter
anti-TuJ1
merge
Pt-HARE5::tdTomato
P
E10.5
Q
R
Hs-HARE5::EGFP
S
T
U

Figure S2, Related to Figure 2. ***HARE5* activity in the lateral telencephalon.** (A-C) Rostral to caudal coronal sections from E10.5 *Hs-HARE5*::*LacZ* brains depicting LacZ activity in the lateral telencephalon with a graded dorso-ventral boundary. (D) Comparison of rostro-caudal matched coronal sections from *Hs-HARE5*::*LacZ* and *Pt-HARE5*::*LacZ* E10.5 embryos. Arrows indicate boundary of uniform LacZ activity and arrowheads indicate boundary of graded LacZ activity. (E-H) Immunofluorescence of E12.5 coronal sections co-expressing *Pt-HARE5*::*tdTomato* and *Hs-HARE5*::*EGFP* at low magnification (E,F) and high-magnification along the lateral wall (G,H), and stained with anti-RFP (E, G) and anti-EGFP (F,H). Note both reporters are active in the VZ/SVZ of the lateral telencephalon. (I-U) Immunofluorescence of E10.5 coronal sections co-expressing *Pt-HARE5::tdTomato* (I-K; P-R) and *Hs-HARE5::EGFP* (L-N; S-U) and stained with anti-RFP (I,P), anti-EGFP (L,S), anti-Pax6 (J,K,M,N) or anti-TuJ1 (Q,R,T,U). Note, *Hs-HARE5* and *Pt-HARE5* activity are high in Pax6-positive neuroepithelial cells but are also evident in some TuJ1-positive neurons. (O) Graph depicting fraction of all Pax6-positive cells that co-stain for either RFP (*Pt*) or EGFP (*Hs*). Note td-Tomato was recognized by anti-RFP. Error bars, s.d. ns, not significant. Scale bars, 100 μm (A-F), 20 μm (G,H), 25 μm (I-N, P-U).

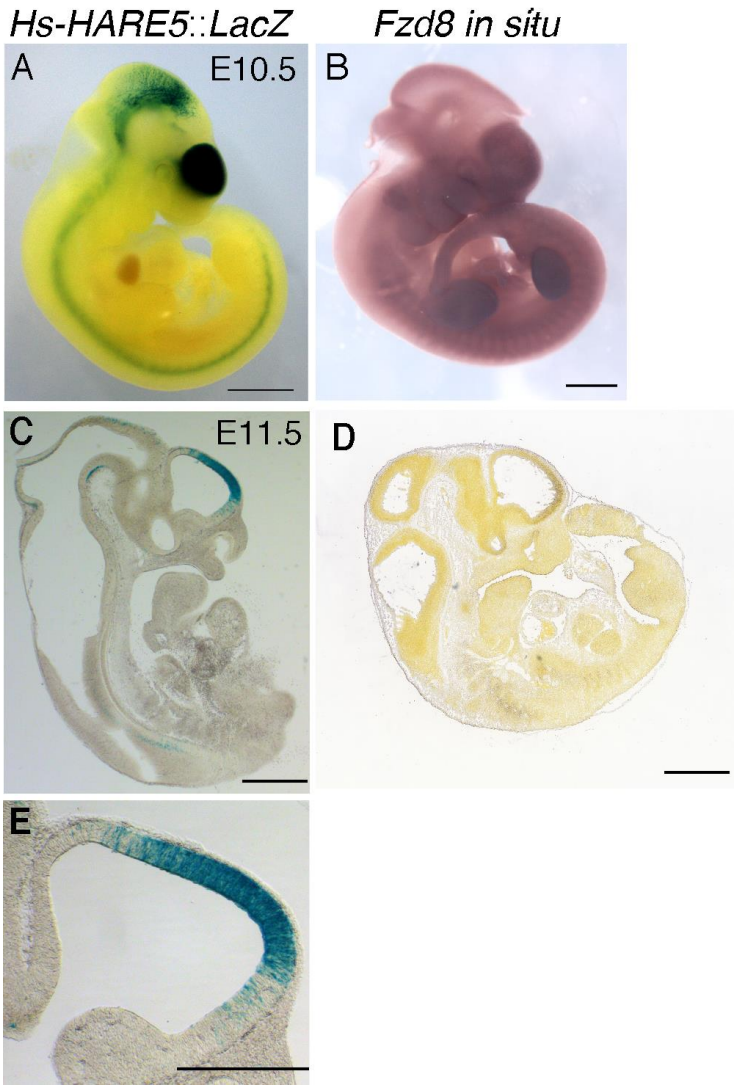

Figure S3, Related to Figure 3. **Hs-*HARE5* activity and mouse *Fzd8* mRNA expression.** (A-E) E10.5 whole mount lateral views (A,B) and E11.5 sagittal sections (C-E) from *Hs-HARE5*::*LacZ* embryo stained for LacZ activity (A,C,E) or for *in situ* hybridization of mouse *Fzd8* mRNA (B,D). *In situ* images are from www.emouseatlas.org [S6] (B), and http://developingmouse.brain-map.org (D). Note *Hs-HARE5* and *Mm-HARE5* share 51.1% sequence identity, as typical for highly conserved noncoding loci [S2, S3]. (E) High magnification image of *Hs-HARE5*::*LacZ* stained section in C. Scale bars, 1 mm (A-D) 590 μm (E).

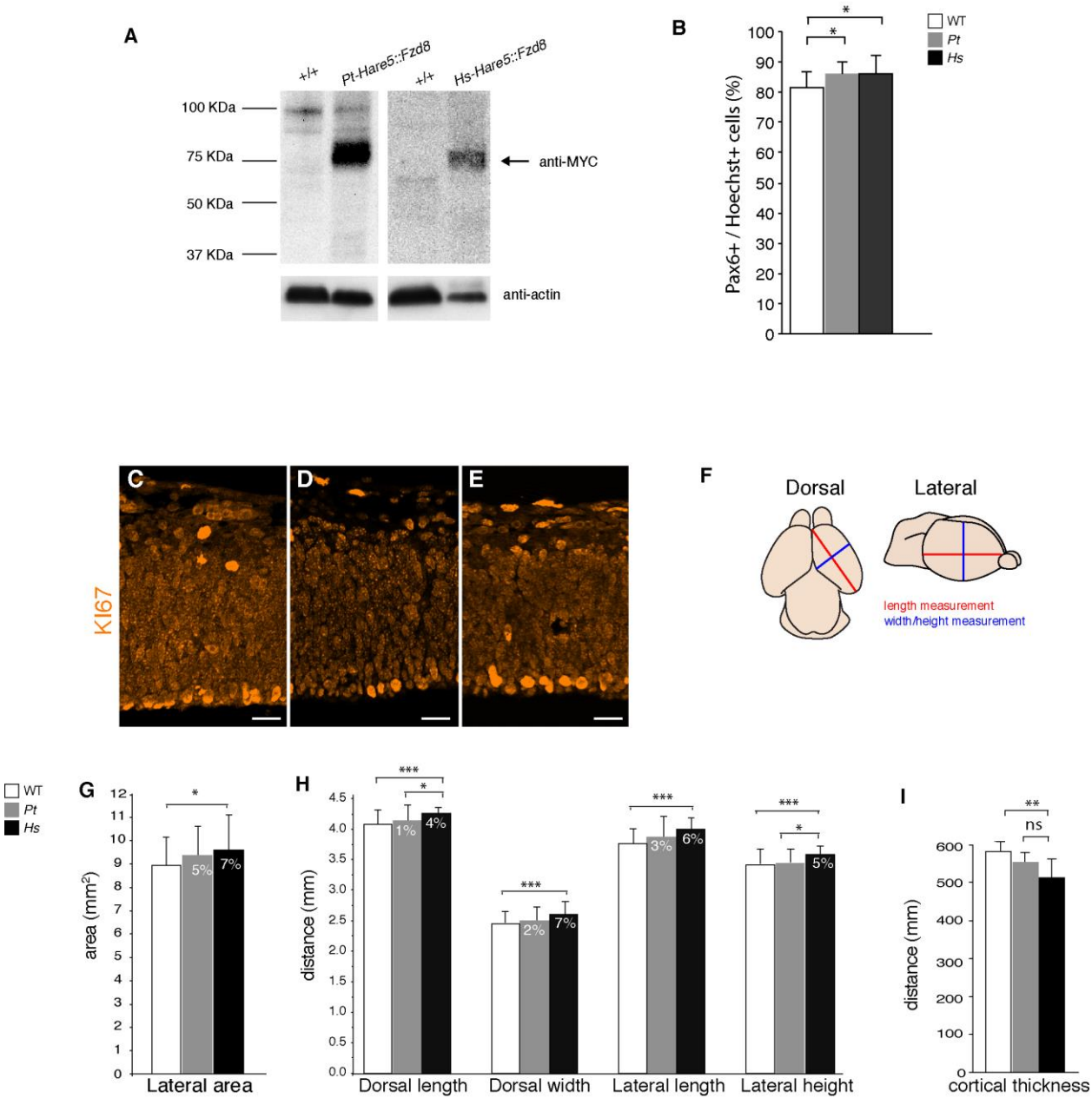

Figure S4, Related to Figure 4. Analysis of *Pt-HARE5::Fzd8* and *Hs-HARE5::Fzd8* brains. (A) Representative western blot of cortices from *Pt-HARE5::Fzd8* and its control littermate (E11.5) and *Hs-HARE5::Fzd8* and its control littermate (E12.5). A 10% SDS-PAGE gel was probed for anti-MYC and anti-Actin, for a loading control. Note a major band of 75KDa evident in both transgenic samples but not in control samples. No significant difference in MYC levels was detected amongst various samples in replicate

westerns. (B) Graph depicting quantification of Pax6-positive cells in control (white box), *Pt-HARE5*::*Fzd8* (gray box), and *Hs-HARE5*::*Fzd8* (black box) brains. (C-E) Coronal E12.5 sections stained for Ki67. (F) Cartoon representation of E18.5 brains with indicated measurements for G,H shown. (G,H) Graphs depicting measurements of E18.5 whole mount brains of indicated genotypes. Note *Hs-HARE5*::*Fzd8* cortices trended to be larger across all measurements, with significance indicated. Included in the bars are the fold increases above WT levels. (I) Graph depicting measurement of coronal sections from E18.5 neocortices of indicated genotypes. Scale bars, C-E, 25 μm. Error bars, s.d., *, $P < 0.05$, **, $P < 0.01$, *** $P<0.001$, ns, not significant.

Epigenetic datasets	Epigenetic mark	P300	Pax6	Sox2	H3K4me1	H3K27ac
	Tissue	E11.5 forebrain [S5]	E12.5 cortex [S9]	E12.5 Neural stem cells [S10]	Neural progenitors [S11]	Neural progenitors [S4]
	# Loci (hg19)	2949	2433	8301	47,258	8,735
Human-accelerated datasets	Prabhakar [S1]	10	0	2	24	4
	Bird [S2]	19	1	2	22	3
	Pollard [S12]	1	0	0	1	0
	Lindblad-Toh (human-accelerated) [S3]	6	0	3	10	0
	Lindblad-Toh (primate-accelerated) [S3]	3	0	4	6	4
Summary	Total intersections (some overlap)	39	1	11	63	11

Table S1. Identification of human/primate-accelerated loci with enhancer marks from *in silico* screen. Related to Figure 1.

Table S2. Transcription factor prediction analysis. Related to Figure 2.

Hs-HARE5 gained binding sites for myc (#1,8,15), a positive regulator of neural stem cell proliferation [S7], and lost binding sites for myc repressors (#8,15), including 2 human-derived and 1 chimpanzee-derived mutations. *Hs-HARE5* lost binding sites for Lef/Tcf (#1,9), which mediates repressor activity in the absence of Wnt signaling, both in human-derived mutations [S8].

Genotype	**Tc (hr)**	**Ts (hr)**	**Tc-Ts (hr)**
WT	12.01 $\pm$ 0.73	6.23 $\pm$ 0.29	5.78 $\pm$ 0.83
Pt	12.15 $\pm$ 1.14	6.34 $\pm$ 0.96	5.81 $\pm$ 0.65
Hs	9.15 $\pm$ 0.88	4.61 $\pm$ 0.41	4.45 $\pm$ 0.65
P-value Hs vs WT	$1.5x10^{-4}$	$2x10^{-5}$	0.016
P-value Hs vs Pt	$1.4x10^{-4}$	0.001	0.003

Table S3. Analysis of cell-cycle kinetics in WT and transgenic E12.5 embryos.

Related to Figure 4.

Supplemental Experimental Procedures

Bioinformatics and *in silico* screen

We propose the term human-accelerated regulatory element (*HARE*) to denote loci that have been bioinformatically identified as rapidly evolving in humans and empirically demonstrated as *in vivo* enhancers. We identified putative *HAREs* from an *in silico* screen using the following approach (outlined in Figure S1A). Enhancer candidate loci were obtained from publicly available datasets containing empirically identified enhancers. These were derived from ChIP-seq studies of mouse embryonic neocortical tissue or

neural stem cells including: p300 [S5], PAX6 [S9], SOX2 [S10], H3K4me1 [S11] and H3K27ac [S4]. We then identified regions of overlap between these enhancer loci and human-accelerated noncoding regions derived from published datasets [S1-3, S12]. All human genomic intervals were then converted to hg19 with the Convert Genome Coordinates tool (v1.0.3) using default settings. Mouse genomic intervals (mm9) were converted to orthologous human coordinates (hg19) with the Extract Pairwise MAF blocks tool (1.0.1) using default settings. MAF blocks were then converted to the BED format using the Maf to BED tool (v.1.0.0) under default parameters. Intersections between human enhancer regions mapped from the mouse genome and human non-coding accelerated regions were determined using the Intersect tool (v.1.0.0) with at least a 1 bp of overlap. Phylogenetic analysis of the *HARE5* locus was performed with MEGA (v5.2.1)[13] on orthologous *HARE5* loci obtained from the UCSC Genome Browser Convert to New Genome tool. We constructed a maximum likelihood tree using the Hasegawa-Kishino-Yano model and a gamma distribution of rates among sites with 5 discrete categories. We utilized the Galaxy Project platform for analyzing genomic datasets [S14].

Sub-cloning of transgenic constructs

For all reporter constructs, enhancer loci were amplified from human genomic DNA (GM12154) and chimpanzee (#5006007) genomic DNA using Phusion High Fidelity Polymerase and directionally cloned into the Gateway entry vector pENTR/D-TOPO (Invitrogen) following the manufacturer's recommendations. DNA reporter constructs were generated containing the original human-accelerated locus, and flanking 5' and 3'

sequences, which have been shown to have accessory regulatory motifs required for enhancer activity [S15-17]. Clones were then subcloned into the minimal promoter *hsp68*::LacZ destination vector (kind gift of Len Pennacchio, Lawrence Berkeley National Laboratory). We generated new fluorescent reporter constructs by modifying the minimal promoter *hsp68*::3nls-*CFP-PEST* vector (generous gift from Jèròme Collignon, Universitè Paris-Diderot). The 3xNLS (nuclear localization sequence) was removed by first amplifying the *CFP* gene without the 3xNLS using primers engineered with BamHI (including a Kozak sequence and the first 5 codons of *CFP*) and a BlpI restriction site positioned upstream and downstream, respectively, of the reporter gene. The plasmid was then digested with BamHI and BlpI restriction enzymes, which removed both the 3xNLS and *CFP* reporter, and re-ligated back together with the PCR amplified *CFP* gene lacking the 3xNLS. We subsequently replaced the *CFP* reporter gene with PCR amplified *tdTomato* and *EGFP* genes engineered with BamHI and BlpI restriction sites. Enhancer loci were subcloned into the multiple cloning site of either *hsp68*::*EGFP-PEST* or *hsp68*::*tdTomato-PEST*. Reporter constructs *Hs-HARE5-hsp68*::*EGFP-PEST* (linearized with XbaI, XhoI, and SalI-HF) and *Pt-HARE5-hsp68*::*tdTomato-PEST* (linearized with XhoI, DraIII, and BstB1) were purified by gel electrophoresis. We generated *Hs-HARE5::Fzd8* and *Pt-HARE5::Fzd8* constructs by first synthesizing mouse *Fzd8* cDNA downstream of the proximal promoter region of hsp68 flanked by XhoI and XbaI restriction sites (GenScript). This cassette was transferred to pCAG using XhoI/XbaI and *Hs/Pt-HARE5* was subcloned with XhoI and EcoNI. All DNA sequences used for transgenic generation were fully sequenced.

Identification of putative transcription factor (TF) binding sites in *HARE5*

To identify potential TF binding sites, we used *in vitro* DNA binding specificity data generated using universal protein-binding microarray (PBM) assays [S18]. PBM data can be used to derive TF-DNA binding motifs, but in addition it yields measurements of TF binding specificity for all possible 8-bp sequences (8-mers), thus providing a more comprehensive view of TF binding preferences compared to DNA motifs. The relative binding preference of a TF for each 8-mer on universal PBMs is quantified by the PBM enrichment score (E-score) [S18, S19] . The E-score is a modified form of the Wilcoxon-Mann Whitney statistic and ranges from -0.5 (least favored sequence) to +0.5 (most favored sequence), with values above 0.35 corresponding, in general, to sequence-specific DNA binding of the tested TF [S18]. We used 612 uPBM data sets for human and mouse TFs from the UniPROBE database and other resources [S20-23]. For each PBM data set, we scanned both the human and the chimpanzee enhancers to identify putative TF binding sites, defined as sites containing at least two consecutive 8-mers with E-score > 0.35, similarly to the procedure used in [S24]. Next, we focused on the specific mutations in the *HARE5* locus, and we identified TFs for which: 1) a putative binding site was predicted in only one of the two lineages, and 2) the difference in E-score between the human and the chimpanzee site was at least 0.2. The selected TFs were used in the analyses presented in the Table S3.

Mouse genetics and embryonic analysis

All experiments were performed in agreement with the relevant regulatory standards from the Division of Laboratory Animal Resources and IACUC at Duke University School of Medicine. DNA for pronuclear injection was prepared by digesting fully constructs with

XhoI/XbaI/SalI-HF (NEB) and purified by electrophoresis (QiaEX II, Qiagen). All linearized constructs were submitted to the Duke Transgenic Mouse Facility for pronuclear injection into 6SJLF1/J strain blastocysts. For the initial screen transient transgenics were tested for enhancer activity using a standard enhancer assay for β-Galactosidase activity. This approach can capture spatial and temporal differences in enhancer function (see [S25, S26] for relevant discussion). For all analyses of *HARE5,* following pronuclear injection, 6SJLF1/J founders were backcrossed to B6/J for subsequent analysis and line propagation. The following lines were generated, with number of lines used shown in parentheses: *Pt-HARE5::LacZ* (3), *Hs-HARE5::LacZ* (4), *Pt-HARE5*::*tdTomatoPEST* (3), *Hs-HARE5*::*EGFP-PEST* (3), *Pt-HARE5*::*Fzd8* (3), and *Hs-HARE5*::*Fzd8* (3). All analyses of enhancer LacZ activity, fluorescence activity, and functional analyses were performed blindly with respect to genotype, and by multiple investigators.

Imaging and immunofluorescence staining of transgenics

LacZ enhancer activity was detected as previously described [S15, S27]. Images of whole-mount LacZ or fluorescent embryos were obtained on a Leica M165 FC microscope using the Leica Application Suite software package (v.4.1.0). For sectioning LacZ embryos, previously fixed embryos were washed in 1X PBS, incubated overnight in 30% sucrose and then embedded in OCT. For sectioning all other embryos, mouse embryos were fixed in 4% paraformaldehyde for 2 hrs. at room temperature or overnight at 4^{o}C and washed 3 x 5 min in 1X PBS solution before an overnight incubation with 30% sucrose at 4^{o}C prior to OCT embedding. Tissue sections were cut 20 µm thick on a cryostat and transferred to Super-Frost Plus slides (Thermo Scientific). Tissue sections

were permeabilized with 0.25% triton-X100 in PBS, stained in primary antibodies for 2 hr. at room temperature or overnight at 4^{o}C as previously described [S28] using the following antibodies: mouse anti-TuJ1 (Covance, 1:400), rabbit anti-Pax6 (Millipore, 1:1,000), mouse anti-Pax6 (DSHB, 1:64), mouse anti-MYC (Cell Signaling, 1:200), rabbit anti-Ki67 (Abcam, 1:200), rabbit anti-RFP (Rockland, 1:400), rabbit anti-Foxp1 (Abcam, 1:200), rabbit anti-Foxp2 (Abcam, 1:1000), and chicken anti-EGFP (Abcam, 1:200). EdU stained sections were obtained using Click-iT EdU Alexa Fluor 594 Imaging Kit (Invitrogen) using manufacturer specifications. Fluorescent images were collected on a Zeiss Observer Z1 microscope using ApoTome optical sectioning. Images of native fluorescent proteins were acquired using the Zeiss 43 HE DsRed (Excitation: 545/15) and 38 HE Green Fluorescent (Excitation: 470/40) and Leica GFP3 ET (Excitation: 470/40) and DSR ET (Excitation: 545/30) filter sets.

RT-qPCR Analysis

RNA was extracted from microdissected E10.5 mouse neocortices stored in TRI reagent (Sigma, Cat #T9424) and stored at -80˚C. RNA was extracted according to manufacturer recommendations. RNA samples were treated with DNaseI and cDNA was synthesized with iScript cDNA Synthesis Kit (Bio-Rad, Cat # 170-8891). qPCR was performed using FastStart Universal SYBR Green Master (Rox) (Roche Applied Science Cat # 04913922001) or Fast SYBR Green Master Mix (Applied Biosystems, Cat # 4385612) using cycling conditions recommended by the manufacturer on an ABI StepOnePlus Real-Time PCR machine. Primers (see Table S4) for tdTomato and EGFP were designed

using Primer3 (v.0.4.0) in order to produce similarly sized amplicons under identical cycling conditions. Similar amplification efficiencies for both primer sets were obtained.

Chromosomal Confirmation Capture (3C) Analysis

3C assays were performed as previously described [S29]. Embryonic neocortices and reference liver tissues were obtained from pools of 10-16 E12.5 embryos. Neocortical dissections included both the dorsal and ventral telencephalon. Tissue samples were dissociated in 0.125% collagenase type I shaking for 1-2 hr. at 37˚C and fixed with 2% formaldehyde/10%FBS/PBS for 10 min at room temperature. Cell nuclei were prepared from aliquots of 10 million cells and stored at -80˚C until chromatin preparation. Cell nuclei were digested with HindIII (New England BioLabs) overnight and re-ligated with T4 DNA ligase-HC (Promega) for 1-2 days. Control template DNA for quantification of 3C ligation products and normalization was generated from HindIII digested and re-ligated BAC DNA covering the mouse *HARE5* (RP23-137B19; CHORI), *mFzd8* (RP23-292B21; CHORI), and *Ercc3* (RP23-148C24; CHORI) internal control locus. Re-ligation events from chromatin and BAC DNA preparations were detected using TaqMan Gene Expression Master Mix (Applied Biosystems) and double-dye labeled oligonucleotide probes (PrimeTime Integrated DNA Technologies). All reactions were performed in quadruplicate. Quantification of ligation events were determined from standard curves of re-ligated BAC DNA covering the locus of interest and normalized against the internal control *Ercc3* locus. Measurements are reported from at least four biological replicates.

Cell cycle analysis and quantitation

Analysis of cell-cycle kinetics was performed as previously described [S30, S31]. Briefly, pregnant dams were injected with BrdU at T=0 (70 μg/g of body weight), EdU (10 μg/g of body weight) at T=1.5 hours, and sacrificed at T=2 hrs. Embryos were immediately fixed in 4% paraformaldehyde overnight, and embedded in OCT, and then cryosectioned. For detection of BrdU, samples were citrate boiled (Vector Laboratories, Cat H-3300) for at least 30 min at 98^{o}C and then incubated 2 hrs with rat anti-BrdU (1:200, Abcam) followed by addition of secondary anti-rat (1:400, Molecular Probes). Detection of EdU was performed after secondary antibody incubation under conditions specified by the manufacturer (Life Technologies, Click-iT 594 or 647). Calculation of total cell cycle length (Tc) and length of S phase (Ts) were performed as follows: the portion of cells actively in the S-phase cells (S cells) was determined from the number of EdU+ cells, the leaving fraction (L cells) was determined by the number of BrdU+/EdU- cells, the total number of proliferating cells (P cells) was determined by Ki67+ cells (1:100). Quantification of all cell cycle parameters were determined with at least 5 nonconsecutive slides stained for each marker and were counted blind to genotype using ImageJ software. Quantification of Foxp1 and Foxp2 neurons and Pax6 progenitors was performed using radial columns of coronal cortical sections counted with Image J software. For E18.5 brains, images of E18.5 embryos were captured using a Leica M165 FC microscope with the Leica Application Suite software package (v.4.1.0). Quantitation of tangential length (the distance between posterior and anterior boundaries of the ventricle in sagittal sections), cortical thickness (measured in coronal sections), and whole mount cortical measurements were performed using ImageJ (v1.48s). Measurements were made blind to genotype.

Western blotting

Cortical protein samples and Western blotting were performed as previously shown, with the following exception, per suggestion of Dr. Hiro Matsunami [S28]. In order to resolve and have optimal transfer of the membrane protein, gels were transferred overnight in cold at 16 volts, and samples in SDS-Page buffer were not boiled but instead warmed at room temperature for 2 hours. Blots were probed with mouse anti-Myc (Cell Signaling, 1:1000) and mouse anti-actin (Sigma, 1:200).

HARE Primers	
HARE1.F	CACCCCACTCACTCCACAAGCATC
HARE1.R	GAATTGCCACTTCTCTCCACA
HARE2.F	CACCTCTCCCCAGTTGGATAGAGTAA
HARE2.R	ACCACACTTGAGGCTCTGGA
HARE3.F	CACCTGACCAAGACAGAAGGGAAAA
HARE3.R	ATTTGCTTGGAAAAAGAACCA
HARE4.F	CACCGACATGCACTCTCCTCTCCTG
HARE4.R	AGGGAGACTGATTTTCAAGCA
HARE5 .F	CACCCACAGAGGTTGGGGCACA
HARE5.R	CCAGTGGAAGGCGATAAGAG
HARE6.F	CACCGGGAGAAGGAAAAACGAAGG
HARE6.R	TATTGCTTGAATTGCCCAAAC
Sub cloning Primers	
CFP.BamHI	ATTAGGATCCGCCACCATGGTGAGCAAGGG
CFP.BlpI	AGCCATGGCTAAGCTTCTTGTACAGCTC
td.tomato.BamHI	ATTAGGATCCAGCCACCATGGTGAGCAAGGG
td.tomato.BlpI	GCATGATGCTAAGCTTGACGGTCCGCTTGTACA
EGFP.BamHI	ATTAGGATCCAGCCACCATGGTGAGCAAGGGC
EGFP.BlpI	CCATGGCTAAGCAATCTAGATCCGGTGGA
RT-qPCR Primers	
tdTomato.F	ACCATCGTGGAACAGTACGAG
tdTomato.R	CTTGAAGCGCATGAACTCTTT

EGFP.F	GAAGCAGCACGACTTCTTCAA
EGFP.R	AAGTCGATGCCCTTCAGCTC
GAPDH.R	ACCACAGTCCATGCCATCAC
GAPDH.R	CACCACCCTGTTGCTGTAGCC
3C Primers	
Ercc3.F	GCCCTCCCTGAAAATAAGGA
Ercc3.R	GACTTCTCACCTGGGCCTACA
Mm-HARE5 constant	AGTCTGAGCACCAAATTCAGG
Mm-Fzd8.Test1	TCCTTTCAGACACAAGCATAAG
Mm-Fzd8.Test2	GATGGATTTCCAGAGTGGTTG
Mm-Fzd8.Test3	TTGGCCTTTGTTCTACTTGAG
Mm-Fzd8.Test4	CAAAGAGAAGTTTGAACAAGCA
Mm-Fzd8.Test5	GGCACAGAAAAATGGAGAAAT
Mm-Fzd8.Test6	TTGACAGTGTCCTTTGCCTTA
3C TaqMan Probes	
Mm-HARE5	AAATGAATTATTTTCCAAGTTGAATCA-BQH
Ercc3	AAAGCTTGCACCCTGCTTTAGTGGCC-BQH

Table S4. List of primers used. Related to Experimental procedures.

Supplemental References

S1. Prabhakar, S., Noonan, J. P., Pääbo, S., and Rubin, E. M. (2006). Accelerated

evolution of conserved noncoding sequences in humans. Science *314*, 786.

S2. Bird, C. P., Stranger, B. E., Liu, M., Thomas, D. J., Ingle, C. E., Beazley, C., Miller, W., Hurles, M. E., and Dermitzakis, E. T. (2007). Fast-evolving noncoding sequences in the human genome. Genome Biol *8*, R118.

S3. Lindblad-Toh, K., Garber, M., Zuk, O., Lin, M. F., Parker, B. J., Washietl, S., Kheradpour, P., Ernst, J., Jordan, G., Mauceli, E., et al. (2011). A high-resolution map of human evolutionary constraint using 29 mammals. Nature *478*, 476–482.

S4. Creyghton, M. P., Cheng, A. W., Welstead, G. G., Kooistra, T., Carey, B. W., Steine, E. J., Hanna, J., Lodato, M. A., Frampton, G. M., Sharp, P. A., et al. (2010). Histone H3K27ac separates active from poised enhancers and predicts developmental state. Proceedings of the National Academy of Sciences *107*, 21931–21936.

S5. Visel, A., Blow, M. J., Li, Z., Zhang, T., Akiyama, J. A., Holt, A., Plajzer-Frick, I., Shoukry, M., Wright, C., Chen, F., et al. (2009). ChIP-seq accurately predicts tissue-specific activity of enhancers. Nature *457*, 854–858.

S6. Summerhurst, K., Stark, M., Sharpe, J., Davidson, D., and Murphy, P. (2008). 3D representation of Wnt and Frizzled gene expression patterns in the mouse embryo at embryonic day 11.5 (Ts19). Gene Expression Patterns *8*, 331–348.

S7. Kerosuo, L., Piltti, K., Fox, H., Angers-Loustau, A., Hayry, V., Eilers, M., Sariola, H., and Wartiovaara, K. (2008). Myc increases self-renewal in neural progenitor cells through Miz-1. J Cell Sci *121*, 3941–3950.

S8. Freese, J. L., Pino, D., and Pleasure, S. J. (2010). Wnt signaling in development and disease. Neurobiology of Disease *38*, 148–153.

S9. Sansom, S. N., Griffiths, D. S., Faedo, A., Kleinjan, D.-J., Ruan, Y., Smith, J., van Heyningen, V., Rubenstein, J. L. R., and Livesey, F. J. (2009). The level of the transcription factor Pax6 is essential for controlling the balance between neural stem cell self-renewal and neurogenesis. PLoS Genet *5*, e1000511.

S10. Engelen, E., Akinci, U., Bryne, J. C., Hou, J., Gontan, C., Moen, M., Szumska, D., Kockx, C., van IJcken, W., and Dekkers, D. H. (2011). Sox2 cooperates with Chd7 to regulate genes that are mutated in human syndromes. Nature Publishing Group *43*, 607–611.

S11. Meissner, A., Mikkelsen, T. S., Gu, H., Wernig, M., Hanna, J., Sivachenko, A., Zhang, X., Bernstein, B. E., Nusbaum, C., Jaffe, D. B., et al. (2008). Genome-scale DNA methylation maps of pluripotent and differentiated cells. Nature *454*, 766–770.

S12. Pollard, K. S., Salama, S. R., King, B., Kern, A. D., Dreszer, T., Katzman, S., Siepel, A., Pedersen, J. S., Bejerano, G., Baertsch, R., et al. (2006). Forces shaping the fastest evolving regions in the human genome. PLoS Genet *2*, e168.

S13. Tamura, K., Peterson, D., Peterson, N., Stecher, G., Nei, M., and Kumar, S. (2011). MEGA5: molecular evolutionary genetics analysis using maximum likelihood, evolutionary distance, and maximum parsimony methods. Mol. Biol. Evol. *28*, 2731–2739.

S14. Goecks, J., Nekrutenko, A., Taylor, J., Galaxy Team (2010). Galaxy: a comprehensive approach for supporting accessible, reproducible, and transparent computational research in the life sciences. Genome Biol *11*, R86.

S15. Prabhakar, S., Visel, A., Akiyama, J. A., Shoukry, M., Lewis, K. D., Holt, A., Plajzer-Frick, I., Morrison, H., FitzPatrick, D. R., Afzal, V., et al. (2008). Human-Specific Gain of Function in a Developmental Enhancer. Science *321*, 1346–1350.

S16. Bae, B.-I., Tietjen, I., Atabay, K. D., Evrony, G. D., Johnson, M. B., Asare, E., Wang, P. P., Murayama, A. Y., Im, K., Lisgo, S. N., et al. (2014). Evolutionarily dynamic alternative splicing of GPR56 regulates regional cerebral cortical patterning. Science *343*, 764–768.

S17. Capra, J. A., Erwin, G. D., McKinsey, G., Rubenstein, J. L. R., and Pollard, K. S. (2013). Many human accelerated regions are developmental enhancers. Philosophical Transactions of the Royal Society B: Biological Sciences *368*, 20130025.

S18. Berger, M. F., Philippakis, A. A., Qureshi, A. M., He, F. S., Estep, P. W., and Bulyk, M. L. (2006). Compact, universal DNA microarrays to comprehensively determine transcription-factor binding site specificities. Nat. Biotechnol. *24*, 1429–1435.

S19. Berger, M. F., and Bulyk, M. L. (2006). Protein binding microarrays (PBMs) for rapid, high-throughput characterization of the sequence specificities of DNA

binding proteins. Methods Mol Biol *338*, 245–260.

S20. Robasky, K., and Bulyk, M. L. (2011). UniPROBE, update 2011: expanded content and search tools in the online database of protein-binding microarray data on protein-DNA interactions. Nucleic Acids Res *39*, D124–8.

S21. Weirauch, M. T., Cote, A., Norel, R., Annala, M., Zhao, Y., Riley, T. R., Saez-Rodriguez, J., Cokelaer, T., Vedenko, A., Talukder, S., et al. (2013). Evaluation of methods for modeling transcription factor sequence specificity. Nat. Biotechnol. *31*, 126–134.

S22. Gordân, A. M. A. R. (2013). Distinguishing between Genomic Regions Bound by Paralogous Transcription Factors. 1–13.

S23. Gifford, C. A., Ziller, M. J., Gu, H., Trapnell, C., Donaghey, J., Tsankov, A., Shalek, A. K., Kelley, D. R., Shishkin, A. A., Issner, R., et al. (2013). Transcriptional and epigenetic dynamics during specification of human embryonic stem cells. Cell *153*, 1149–1163.

S24. Gordân, R., Shen, N., Dror, I., Zhou, T., Horton, J., Rohs, R., and Bulyk, M. L. (2013). Genomic regions flanking E-box binding sites influence DNA binding specificity of bHLH transcription factors through DNA shape. CellReports *3*, 1093–1104.

S25. Hubisz, M. J., and Pollard, K. S. (2014). Exploring the genesis and functions of Human Accelerated Regions sheds light on their role in human evolution. Curr Opin Genet Dev *29C*, 15–21.

S26. Enard, W. (2014). Mouse models of human evolution. Curr Opin Genet Dev *29C*, 75–80.

S27. Silver, D. L., Hou, L., Somerville, R., Young, M. E., Apte, S. S., and Pavan, W. J. (2008). The secreted metalloprotease ADAMTS20 is required for melanoblast survival. PLoS Genet *4*, e1000003.

S28. Silver, D. L., Watkins-Chow, D. E., Schreck, K. C., Pierfelice, T. J., Larson, D. M., Burnetti, A. J., Liaw, H.-J., Myung, K., Walsh, C. A., Gaiano, N., et al. (2010). The exon junction complex component Magoh controls brain size by regulating neural stem cell division. Nat Neurosci *13*, 551–558.

S29. Hagège, H., Klous, P., Braem, C., Splinter, E., Dekker, J., Cathala, G., de Laat, W., and Forné, T. (2007). Quantitative analysis of chromosome conformation capture assays (3C-qPCR). Nat Protoc *2*, 1722–1733.

S30. Quinn, J. C., Molinek, M., Martynoga, B. S., Zaki, P. A., Faedo, A., Bulfone, A., Hevner, R. F., West, J. D., and Price, D. J. (2007). Pax6 controls cerebral cortical cell number by regulating exit from the cell cycle and specifies cortical cell identity by a cell autonomous mechanism. Dev Biol *302*, 50–65.

S31. Martynoga, B. S., Morrison, H., Price, D. J., and Mason, J. O. (2005). Foxg1 is required for specification of ventral telencephalon and region-specific regulation of dorsal telencephalic precursor proliferation and apoptosis. Dev Biol *283*, 113–127.